J. Fluid Mech. (2002), *vol.* 471, *pp.* 137–157. © 2002 Cambridge University Press
DOI: 10.1017/S0022112002002136 Printed in the United Kingdom

Magnetohydrodynamic flow in the liquid phase for a specific pool boiling scenario

By LEO BÜHLER

Forschungszentrum Karlsruhe, Postfach 3640, 76021 Karlsruhe, Germany

(Received 19 July 2001 and in revised form 20 June 2002)

In the EVOLVE concept for a nuclear fusion blanket a pool boiling scenario has been proposed where a number of permanent vertical vapour channels are formed in a horizontal layer of liquid lithium. Similar situations occur during laser beam welding where a relatively long vapour capillary is observed. The present analysis focuses on the flow of the electrically conducting liquid phase in the presence of a strong uniform horizontal magnetic field. The cross-section of vapour channels is circular if surface tension dominates magnetic forces. In the opposite case a stretching of the liquid–vapour interface along magnetic field lines is observed and contours become possible where a major part of the interface is straight and aligned with the field. For strong magnetic fields the liquid flow exhibits several distinct subregions. Most of the liquid domain is occupied by inviscid cores. These are separated from each other by parallel layers that spread along the field lines which are tangential to the vapour channel. In one core, which is located between two parallel layers, the flow direction is preferentially oriented along magnetic field lines, while in the other cores the flow is perpendicular to the field.

1. Introduction

Efficient heat removal at high temperatures is a key issue for blankets in nuclear fusion applications. Liquid lithium alloys have been considered in the past as coolant candidates since the composite lithium serves at the same time as a breeding material for generation of tritium. However, the strong braking of the flow by the interaction of the electrically conducting fluid with the magnetic field confining the fusion plasma reduces the heat transfer capabilities of liquid-metal-cooled devices and makes the exclusive use of liquid metals as coolant and breeder less attractive.

The EVOLVE (EVaporation Of Lithium and Vapour Extraction) concept is a recently proposed liquid-metal blanket (Abdou & the Apex Team 2001; Anderson *et al.* 2001). In EVOLVE a significant fraction of the fusion power is released in the liquid by nuclear volumetric heating. This heat is removed from the blanket by evaporation of lithium. Since lithium has a large latent heat of vapourization it is possible to remove high heat fluxes while the velocities in the liquid phase can be kept at very small values. This reduces the magnetohydrodynamic (MHD) interactions considerably. Anderson *et al.* (2001) suggests a potential boiling scenario where permanent vertical vapour channels in horizontal layers of liquid lithium are held open by pressure and momentum in the vapour, against the action of gravity and capillary forces which tend to close the vapour channels. The layers of liquid are located on horizontal trays. One vapour channel is schematically shown in figure 1.

We assume that such a boiling scenario exists and we analyse the two-dimensional

https://doi.org/10.1017/S0022112002002136 Published online by Cambridge University Press

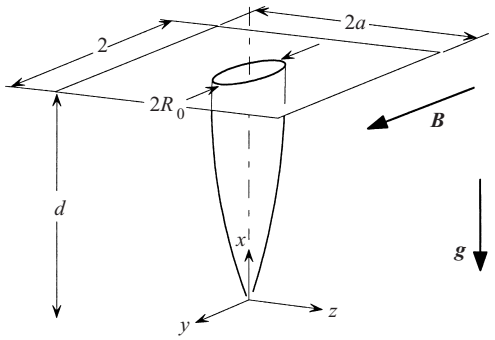


FIGURE 1. Geometry of a vapour channel.

magnetohydrodynamic flow in the liquid phase in a plane perpendicular to these vapour channels. We give estimates for the pressure drop required to drive the liquid to the interface. We show that the shape of the vapour channel cross-section may deviate from the circular one that is expected in the absence of a magnetic field. In case of a horizontal magnetic field the channels are elongated along field lines.

It is not clear that a boiling scenario such as proposed for EVOLVE exists really. This scenario is based on the experience that strong magnetic fields suppress turbulent movements of vapour bubbles, as observed e.g. by Lopez de Bertodano, Leonardi & Lykoudis (1998). They find experimentally that the frequency of rising vapour bubbles first increases with increasing magnetic field but they observe a strong decrease of the bubble frequency with higher magnetic fields. Moreover, they find a complete suppression of the bubble regime for low heat fluxes or for strong magnetic fields. If it is possible to trigger the nucleation sites required for the formation of vapour channels at the strongly heated bottom plate, a boiling scenario could establish that allows sufficient vapour release from the liquid although the velocities in the liquid are small. Stable vapour jets or columns seem possible in non-magnetic boiling if the vapour velocity is below a certain threshold (see e.g. Whalley 1987, pp. 137–139; Dwyer 1976, p. 358). For higher vapour velocities the interface undergoes a Kelvin–Helmholtz instability and becomes wavy and the vapour column finally disintegrates. The application of a magnetic field could stabilize vapour channels and even permit stable regimes beyond the hydrodynamic threshold of stability. The initiation of such a flow pattern and the stability of vapour channels in strong magnetic fields remains to be found.

Note that similar scenarios are observed in laser beam welding, where a relatively long vapour capillary forms around a laser beam. Capillaries with aspect ratios (penetration depth/capillary diameter) up to 25 have been observed in experiments and they are used in engineering applications in order to perform deep penetration welds. Without the formation of capillaries such welds are impossible since the heat input would be restricted to the top surface of the sample which reflects most of the laser light. After a capillary has developed, the reflected light is trapped within the capillary. Multiple reflections occur and each of them absorbs a fraction of the incoming light which is transferred into heat released at the capillary interface. There is current interest in improving the quality of the seams by applying magnetic fields during the welding of aluminium (Tse, Man & Yue 1999; Kern, Berger & Hügel 2000). The results derived below may serve as a basis for a better understanding of the phenomena involved in these processes.

https://doi.org/10.1017/S0022112002002136 Published online by Cambridge University Press

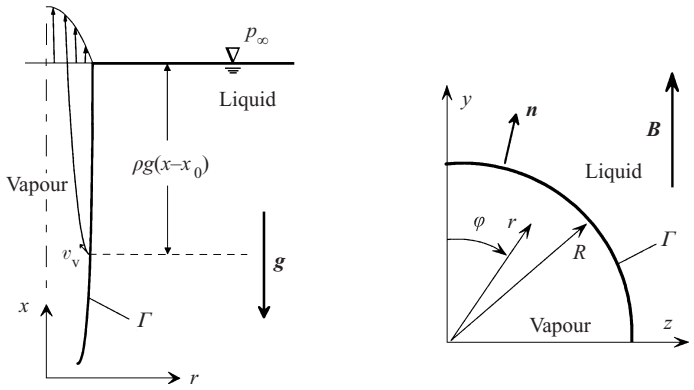


FIGURE 2. Sketch of the geometry and coordinate system in vertical and horizontal cuts though a vapour channel.

2. Formulation

Before we formulate the equations which describe the flow in the liquid phase we consider first the conditions which apply at the interface between the vapour and the liquid, i.e. at an interface with mass transfer. Then we formulate the non-dimensional equations which govern the flow in the liquid phase.

2.1. *Interface conditions*

At the stationary interface Γ between the liquid and the vapour tangential components of velocity are continuous

$$\boldsymbol{v}_\mathrm{v} \times \boldsymbol{n} = \boldsymbol{v} \times \boldsymbol{n}, \tag{2.1}$$

while conservation of mass and momentum requires

$$\rho_\mathrm{v} \boldsymbol{v}_\mathrm{v} \cdot \boldsymbol{n} = \rho \boldsymbol{v} \cdot \boldsymbol{n} \tag{2.2}$$

and

$$\rho_\mathrm{v} \boldsymbol{v}_\mathrm{v} (\boldsymbol{v}_\mathrm{v} \cdot \boldsymbol{n}) - \boldsymbol{n} \cdot \boldsymbol{T}_\mathrm{v} = \rho \boldsymbol{v} (\boldsymbol{v} \cdot \boldsymbol{n}) - \boldsymbol{n} \cdot \boldsymbol{T} + \gamma K \boldsymbol{n}, \tag{2.3}$$

respectively. We may use the following representation of the stress tensor $\boldsymbol{T}$ in terms of the pressure and deformation tensor $\boldsymbol{D}$:

$$\boldsymbol{T}_{(\mathrm{v})} = -p_{(\mathrm{v})} \boldsymbol{I} + 2\rho_{(\mathrm{v})} \nu_{(\mathrm{v})} \boldsymbol{D}_{(\mathrm{v})}. \tag{2.4}$$

In the present notation, γ stands for the surface tension and K is twice the mean curvature, seen from the axis. The quantities ρ, ν and $\boldsymbol{v}$ denote density, kinematic viscosity and velocity in the liquid (without a subscript) and in the vapour (with subscript v). Here, the unit normal $\boldsymbol{n}$ points into the liquid. For a derivation of the interface conditions see e.g. Hsieh (1972). Liquid metals usually have a high thermal conductivity so that the temperature at the liquid–vapour interface can be considered to be uniform with a certain amount of superheating. This yields a mass flux $\rho_\mathrm{v} \boldsymbol{v}_\mathrm{v} \cdot \boldsymbol{n}$ due to evaporation at the interface in order to balance the thermal energy released in the fluid per unit length of the vapour channel by the latent heat of evaporation.

During the analysis we assume for simplicity that variations of the vapour channel geometry along the channel's axis, along x in the present notation, are small. The geometry is sketched in figure 2. In order to justify this assumption we estimate the size and shape of vapour channels for the hydrodynamic case in the Appendix. The simple considerations presented in the Appendix do not prove that slender vapour

https://doi.org/10.1017/S0022112002002136 Published online by Cambridge University Press

capillaries exist but they show that such a scenario is at least plausible. In laser beam welding capillaries called keyholes are observed which are of length more than one order of magnitude greater than their diameter. In electron beam welding processes capillaries are possible which are longer than 10 cm.

2.2. *Governing equations*

In the following analysis we assume in the liquid phase a steady-state flow of a fluid with constant electric conductivity σ for which inertia forces are negligible in comparison with electromagnetic forces. The horizontal magnetic field $\boldsymbol{B} = B\hat{\boldsymbol{y}}$ has a magnitude B and an orientation along the y-coordinate perpendicular to the vapour channel. For details of the geometry and coordinate systems see figure 2.

The governing non-dimensional equations for momentum and Ohm's law then reduce to

$$\nabla p = \frac{1}{Ha^2}\nabla^2 \boldsymbol{v} + \boldsymbol{j} \times \hat{\boldsymbol{y}} - G\hat{\boldsymbol{x}}, \tag{2.5}$$

$$\boldsymbol{j} = -\nabla\phi + \boldsymbol{v} \times \hat{\boldsymbol{y}}. \tag{2.6}$$

There is a balance between pressure forces, viscous forces, Lorentz forces and gravity. The currents of density $\boldsymbol{j}$ are driven by the gradient of a scalar electric potential ϕ and by the induced electric field $\boldsymbol{v} \times \hat{\boldsymbol{y}}$ due to the fluid motion. Conservation of mass and charge requires that

$$\nabla \cdot \boldsymbol{v} = 0, \quad \nabla \cdot \boldsymbol{j} = 0. \tag{2.7}$$

Here, the variables p, ϕ, $\boldsymbol{v}$ and $\boldsymbol{j}$ denote in the liquid phase the pressure, the electric potential, the velocity vector and the electric current density, scaled by the reference quantities $\sigma v_0 B^2 L$, $v_0 B L$, v_0 and $\sigma v_0 B$, respectively. The characteristic velocity v_0 is given by the rate of evaporation at the interface between vapour and liquid and L is a typical length scale of the problem in the plane of the vapour channel's cross-section. For circular vapour channels L would be the radius. For periodically occurring vapour channels L is the half-spacing between neighbouring channels, measured along magnetic field lines.

The square of the Hartmann number

$$Ha = LB\sqrt{\frac{\sigma}{\rho\nu}} \tag{2.8}$$

measures the ratio of electromagnetic forces to viscous forces. For applications in nuclear fusion Ha is typically on the order of 10^3 to 10^4. In the present case the size of the vapour channels L is not as large as the dimensions encountered usually in duct flows, but large enough that the Hartmann number is still very high, $Ha \gg 1$. The parameter

$$G = \frac{\rho g}{\sigma v_0 B^2} \tag{2.9}$$

is a non-dimensional measure of gravitational acceleration. The assumption that inertia is negligible compared to electromagnetic forces is justified for slow motions with typical velocity v_0 for which the interaction parameter N is large, i.e.

$$N = \frac{\sigma L B^2}{\rho v_0} \gg 1. \tag{2.10}$$

We restrict the present analysis to cases which are symmetric with respect to the y-axis. This requires that $w = \partial_z v = \partial_z p = \phi = 0$ at $z = 0$. We consider a typical plane

https://doi.org/10.1017/S0022112002002136 Published online by Cambridge University Press

perpendicular to the channel's axis in which the derivatives of flow variables along x are small compared with the variations in this plane, i.e. $\partial_x \ll \partial_y, \partial_z$. We shall show later in § 4.5 that the potential gradient $\partial_x \phi$ near the vapour channel is proportional to z/d, a quantity which is negligible for slender vapour channels for which $d \gg z$. Therefore

$$\partial_x \phi = 0 + O(z/d) \tag{2.11}$$

is a property which is small, independently of the Hartmann number. Equation (2.11) could be obtained formally by introducing a slow coordinate $X = x/d$, which results in small $\partial_x \phi = O(d^{-1})$ for $d \gg 1$. Moreover, for high Hartmann numbers the currents are uniform along magnetic field lines, i.e. $\partial_y j_y = 0$. This result is based on equation (2.5) and the fact that $\nabla \times (\boldsymbol{j} \times \hat{\boldsymbol{y}})$ is zero at high Hartmann numbers. We find with the symmetry condition at $y = 0$ the result that

$$j_y = -\partial_y \phi = 0. \tag{2.12}$$

From these considerations we conclude that the potential ϕ near the vapour channel is close to zero. Nevertheless, it may vary as a function of x and z at larger distances.

The mass conservation equation is identically satisfied by choosing a streamfunction ψ for velocity as

$$\boldsymbol{v} = v\hat{\boldsymbol{y}} + w\hat{\boldsymbol{z}} = \partial_z \psi \hat{\boldsymbol{y}} - \partial_y \psi \hat{\boldsymbol{z}}. \tag{2.13}$$

Elimination of pressure from (2.5) by taking the curl yields the following equation for the x-component of vorticity $\boldsymbol{\omega} = \nabla \times \boldsymbol{v} = \omega \hat{\boldsymbol{x}}$:

$$\nabla^2 \omega + Ha^2 \partial_y j_x = 0. \tag{2.14}$$

We eliminate the current by Ohm's law (2.6)

$$j_x = -\partial_x \phi - w = \partial_y \psi + O(z/d) \tag{2.15}$$

and finally find

$$\nabla^2 \omega + Ha^2 \partial_{yy} \psi = 0. \tag{2.16}$$

The definition of vorticity expressed in terms of the streamfunction leads to an equation that determines ψ:

$$\nabla^2 \psi + \omega = 0. \tag{2.17}$$

We suppose that the mass flux transferred from the liquid to the vapour phase is uniform along the liquid–vapour interface. This requires a uniform normal component of velocity $\boldsymbol{v} \cdot \boldsymbol{n} = -1$ at Γ, with the unit normal $\boldsymbol{n}$ pointing from the vapour into the liquid. Expressed in terms of the streamfunction this relation is equivalent to

$$\partial_t \psi = -1 \quad \text{at} \quad \Gamma, \tag{2.18}$$

where t is a coordinate along the interface in the (y, z)-plane, with a tangential unit vector $\boldsymbol{t}$. Thus, the streamfunction ψ becomes proportional to the arclength measured along Γ.

If we project the interface condition (2.3) into the tangential direction $\boldsymbol{t}$ and assume that the vapour has no velocity component along $\boldsymbol{t}$, we find $\boldsymbol{n} \cdot \boldsymbol{D} \cdot \boldsymbol{t} = 0$, which is equivalent to

$$\omega = 0 \quad \text{at} \quad \Gamma \tag{2.19}$$

since we supposed a uniform normal component of velocity along the interface. The interface Γ between the vapour and the liquid is free of tangential shear stress in the plane of the liquid motion. The boundary conditions (2.18) and (2.19) are sufficient to

https://doi.org/10.1017/S0022112002002136 Published online by Cambridge University Press

describe the flow for a given contour Γ. However, if the determination of the contour is a part of the solution, we have to consider in addition the normal projection of (2.3) and take into account that the pressure jumps across the interface. The problem is entirely determined if conditions for ψ and ω at infinity or at a finite distance from the interface are known. This point is discussed later in the paper.

3. Numerical solution

In order to obtain a first impression of the structure of the flow we assume that the geometry of the vapour channel remains circular and that the surrounding liquid domain is unbounded. Later we will relax the condition on the interface and allow for non-circular interface geometries which are determined by the solution of the problem. We introduce a polar coordinate system located in the centre of the vapour channel. For a numerical solution of (2.16) and (2.17) it would be desirable both to resolve the Hartmann layer at the liquid–vapour interface and to extend the computational domain to large values of r. For that reason we apply a transformation to the radius such as

$$r = \exp(\xi). \tag{3.1}$$

This transformation gives a good resolution near $r = 1(\xi = 0)$ and, even if $r_{\max} \gg 1$, $\xi_{\max}$ has values of order unity. We multiply the equations by r^2 and find for the Laplacian

$$r^2\nabla^2 = \partial_{\xi\xi} + \partial_{\varphi\varphi} \tag{3.2}$$

and

$$r^2\partial_{yy} = \sin^2\varphi\,\partial_{\varphi\varphi} + \cos^2\varphi\,\partial_{\xi\xi} + 2\sin\varphi\cos\varphi(\partial_\varphi - \partial_{\xi\varphi}) + (\sin^2\varphi - \cos^2\varphi)\partial_\xi. \tag{3.3}$$

To minimize the computational effort we make use of symmetries in the problem. There is no flow across the lines $\varphi = 0$ and $\varphi = \pi/2$ so that it is sufficient to consider only the sector between these lines with symmetry conditions

$$\left.\begin{aligned} &\psi = 0, \qquad \omega = 0 \quad \text{at} \quad \varphi = 0, \\ &\psi = -\tfrac{1}{2}\pi, \quad \omega = 0 \quad \text{at} \quad \varphi = \tfrac{1}{2}\pi. \end{aligned}\right\} \tag{3.4}$$

At the liquid–vapour interface we have according to (2.18) and (2.19)

$$\psi = -\varphi, \quad \omega = 0 \quad \text{at} \quad r = 1. \tag{3.5}$$

It is difficult to formulate a proper condition for the streamfunction as $r \to \infty$. A possibility could be to assume a radial inflow, especially for the case of weak magnetic fields. However, as we shall see below, for high Hartmann numbers the inflow will be more parallel to magnetic field lines than oriented along the radial direction. For strong magnetic fields, $Ha \gg 1$, a more appropriate condition could be to assume an inflow aligned with the magnetic field

$$\partial_y\psi = 0 \quad \omega = 0 \quad \text{as} \quad r \to \infty. \tag{3.6}$$

Computations using this condition at large radii show that the boundary condition does not give a perfect description of the continuous spreading of the solution along z with increasing y. On the other hand, order of magnitude estimations reduce the governing equation (4.2), $-\nabla^4\psi + Ha^2\partial_{yy}\psi = 0$, at larger distance from the interface to

$$-\partial_\zeta^4\psi + \partial_{yy}\psi = 0, \tag{3.7}$$

https://doi.org/10.1017/S0022112002002136 Published online by Cambridge University Press

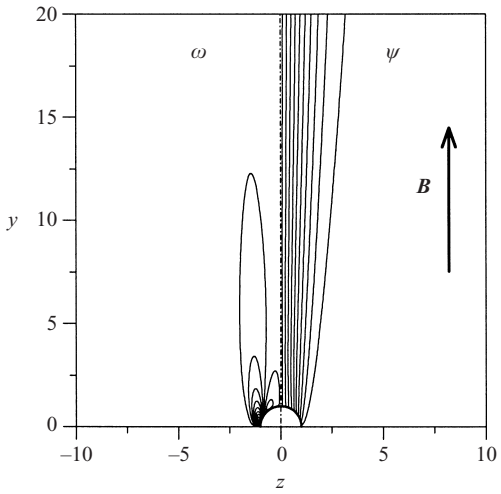


FIGURE 3. Streamlines (right) and isolines of vorticity (left) for a flow towards a circular vapour channel. $Ha = 20$, $r_{\max} = 100$.

where $\zeta = \sqrt{Ha}\, z$ is a stretched transverse coordinate. Such an equation allows self-similar solutions as $\psi(\eta)$, where $\eta = \zeta/\sqrt{y}$. Now we may evaluate $\partial_y \psi = \partial_\eta \psi \partial_y \eta$ and $\partial_z \psi = \partial_\eta \psi \partial_z \eta$ and eliminate $\partial_\eta \psi$ from both equations. This leads to a condition

$$2y\partial_y \psi + z\partial_z \psi = 0, \tag{3.8}$$

or when expressed in terms of the polar coordinates introduced above we find

$$-\sin\varphi\cos\varphi\,\partial_\varphi \psi + (\cos^2\varphi + 1)\,\partial_\xi \psi = 0 \quad \text{as} \quad r, \xi \to \infty. \tag{3.9}$$

For the solution we apply a heat transfer code to solve the problem iteratively using finite difference techniques. A more efficient way, however, could be to use a fast Poisson solver to invert the Laplacians. Numerical calculations are performed on a finite domain which ends at $r_{\max} = 100$ ($\xi_{\max} = 4.6$). A grid with $n_\xi \times n_\varphi = 100 \times 500$ points was used for the calculations for $Ha = 20$ based on the radius of the vapour channel. Calculations with other maximum radii or grids did not show significant differences. The Hartmann layer which appears near $r = 1$ is resolved with a few grid points. For MHD duct flow such a low resolution would be not sufficient since in that case the currents close through the layers so that the layers determine the whole solution. Here, the currents close through the cores in a direction perpendicular to the computational domain. A more complete description of the current paths is given later in § 4.5. The physics is mainly governed by the flow outside the Hartmann layers. The role of the layer is to match the core vorticity with the condition at the interface where $\omega = 0$. The boundary layer for ω is better expressed than the layer for ψ because the wall-normal component of velocity does not change at the leading order across the layer as $Ha \gg 1$.

We show in figure 3 results for $Ha = 20$ based on the radius of the vapour channel. We do not show results for smaller values but describe the phenomena briefly. In the hydrodynamic case when $Ha = 0$, the flow is purely radial. With increasing Hartmann number the streamlines are shifted to a narrow region close to the y-axis where they are mainly parallel and aligned with the magnetic field. Details of the flow near the interface can be seen from figure 4. We see that the vorticity ω develops pronounced Hartmann layers with large gradients near the interface. The streamfunction ψ does

https://doi.org/10.1017/S0022112002002136 Published online by Cambridge University Press

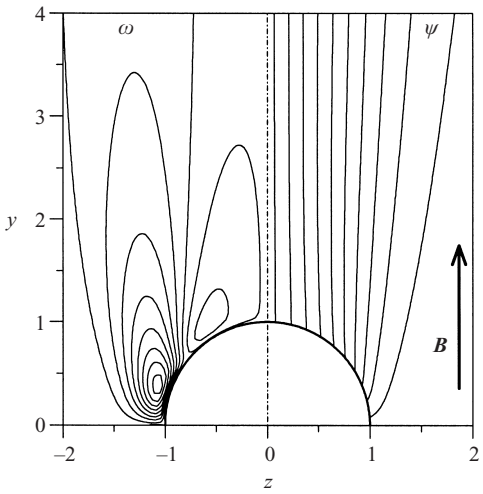


FIGURE 4. Streamlines (right) and isolines of vorticity (left) for a flow towards a circular vapour channel. Enlargement of figure 3.

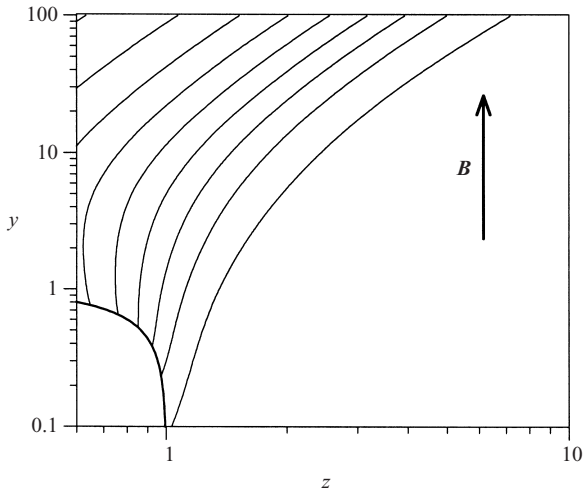


FIGURE 5. Streamlines for a flow towards a circular vapour channel. Data from figure 3 on logarithmic scales to demonstrate the self-similar behaviour as $r \to \infty$.

not show such a behaviour since the fluid approaches the interface along smooth paths. Both figures 3 and 4 show a small fraction of the whole computational domain, which extends to a radius of $r_{\max} = 100$. An overview of the flow in the whole domain is shown in the logarithmic plot in figure 5. The streamlines become straight with a slope of 2 in the far field and confirm the self-similar character of the solution in some distance from the vapour channel.

The interaction with the magnetic field pushes the flow in a direction parallel to the field in order to minimize Lorentz forces. Lorentz forces vanish if the flow is exactly aligned with the field. The above reasoning shows that there are no Lorentz forces along the y-axis or along the z-axis in some distance from the interface. Therefore there is no MHD pressure drop along y and along z because the fluid can flow

https://doi.org/10.1017/S0022112002002136 Published online by Cambridge University Press

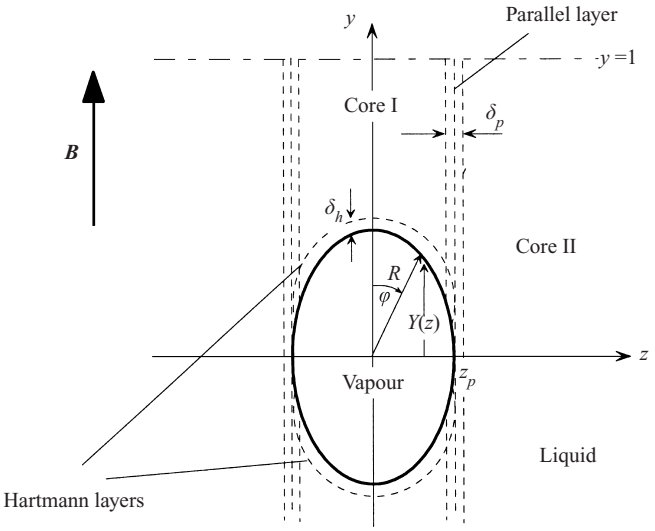


FIGURE 6. Two-dimensional model geometry with flow subregions. Inviscid cores are separated from each other by internal parallel layers. Hartmann layers form near the interface.

towards the interface aligned with the field. This result is a direct consequence of the assumption that the liquid domain has a large extent.

In the next section we consider a case where the liquid domain has a finite extent along y. Such a restriction will force the flow to have a component of velocity perpendicular to the magnetic field, associated with an MHD pressure drop.

4. Asymptotic analysis

In this section we consider the case when the vapour channels occur periodically along y with dimensional distance $2L$ measured along field lines and spacing aL in the transverse direction. The fluid is supplied to the volume considered at the positions $z = \pm aL$. The volumetric heat q given to a volume element of size $dx \times L \times aL$ evaporates the liquid at the interface into the vapour channel. Total heat removal via the vapour channels requires a flow rate

$$\psi_0 = \frac{qaL^2}{\rho H}, \tag{4.1}$$

where H stands for the latent heat of evaporation. Consistent with this flow rate is a typical velocity ψ_0/L far from the capillary. In the two-phase flow literature a characteristic velocity is the superficial vapour velocity v_g (Whalley 1987), which differs from ψ_0/L by the density ratio between the liquid and the vapour phase. The velocity normal to the interface evaluates to $v_0 = \psi_0/l$, where l stands for the arc length along the capillary measured from $\varphi = 0$ to $\varphi = \pi/2$. In the following we use the half-spacing along field lines as a characteristic length scale of the problem and assume that the magnetic field is large enough that the Hartmann layers are thin compared with the radius of the vapour channel. For details of the geometry see figures 1 and 6. The scaling used here differs from that used earlier but it leads to a simpler representation of the results derived below. We are mainly interested in the flow near the vapour–liquid interface and do not consider the question of how the flow is carried towards the lateral borders.

https://doi.org/10.1017/S0022112002002136 Published online by Cambridge University Press

For large Hartmann numbers the flow region splits into distinct subregions. These are for the present case the inviscid cores I and II and the viscous Hartmann and parallel layers. Hartmann layers appear typically at fluid boundaries where a normal component of the magnetic field is present. Parallel layers appear at boundaries which are aligned with the magnetic field or between two inviscid cores. In any case, parallel layers spread along magnetic field lines from singularities at boundaries, for example from corners in duct flows (Hunt & Leibovich 1967) or in the present case from the position where the slope of the contour $\partial_z Y$ is infinite, as shown in figure 6. All these layers are well-known in strong field MHD flows. For more details the reader is referred to classical text books on MHD or to more recent publications like Moreau (1990), Davidson (2001) or Müller & Bühler (2001).

The scales of the viscous layers become clear if we eliminate the vorticity in (2.16) using the streamfunction according to (2.17), which yields

$$-\nabla^4\psi + Ha^2\partial_{yy}\psi = 0. \tag{4.2}$$

In order to describe the flow in the Hartmann layer we consider in more detail the layer which is located at $y = Y$ by using the stretched coordinate $\eta = (y - Y)/\delta_h$ with $\delta_h \ll 1$. This results at leading order in

$$-\frac{1}{\delta_h^4}\partial_\eta^4\psi + Ha^2\frac{1}{\delta_h^2}\partial_{\eta\eta}\psi = 0, \tag{4.3}$$

and an adequate balance of forces in the Hartmann layer determines the typical thickness of the layer as $\delta_h = Ha^{-1}$.

If we stretch the parallel layer at z_p by using the coordinate $\zeta = (z - z_p)/\delta_p$ equation (4.2) becomes at leading order

$$-\frac{1}{\delta_p^4}\partial_\zeta^4\psi + Ha^2\partial_{yy}\psi = 0 \tag{4.4}$$

so that a balance of forces requires $\delta_p = Ha^{-1/2}$. A possible way to solve the flow problem in the parallel layer has been outlined by Garandet, Alboussière & Moreau (1992).

We construct a composite solution for the unknowns such as

$$\left.\begin{aligned}\omega &= \omega_c(y,z) + \omega_h(\eta) + \omega_p(y,\zeta),\\ \psi &= \psi_c(y,z) + \psi_h(\eta) + \psi_p(y,\zeta),\end{aligned}\right\} \tag{4.5}$$

where the subscripts denote the contributions due to the solution in the inviscid cores and in the viscous Hartmann and parallel layers.

4.1. *The Hartmann layers*

We have already seen qualitatively that the role of the Hartmann layers is almost passive since the normal component of velocity does not change significantly across the layer. We shall now support this observation by arguments. We introduce a stretched Hartmann layer coordinate $\eta = Ha\,(y - Y)$, where $Y(z)$ describes the contour of the vapour channel. Then (2.17) simplifies to

$$Ha^2\partial_{\eta\eta}\psi_h + \omega_h = 0, \tag{4.6}$$

and when substituted into the vorticity equation (2.16) we find in the limit as $Ha \to \infty$

$$\partial_{\eta\eta}\omega_h - \omega_h = 0. \tag{4.7}$$

https://doi.org/10.1017/S0022112002002136 Published online by Cambridge University Press

Here, ψ_h and ω_h denote the viscous corrections in the Hartmann layers to the inviscid core solution. The solution for vorticity inside the layer is purely exponential,

$$\omega_h = -\omega_c \exp(-\eta). \tag{4.8}$$

It matches the core solution $\omega_h \to 0$ as $\eta \to \infty$ with the interface condition $\omega_h = -\omega_c$ at $\eta = 0$. The streamfunction ψ_h does not change across the Hartmann layer at leading order of approximation. This can be shown by integration of (4.6) between η and ∞. With the requirement that the viscous corrections vanish as $\eta \to \infty$ we find

$$\psi_h = Ha^{-2}\omega_c \exp(-\eta). \tag{4.9}$$

There is therefore no viscous correction of the streamfunction across the Hartmann layer at leading order so that we can apply the condition at the interface (2.18) directly to the core solution

$$\partial_t \psi_c = -1 \quad \text{at} \quad y = Y. \tag{4.10}$$

4.2. *The core*

In the core equation (2.16) reduces for $Ha \to \infty$ to

$$\partial_{yy}\psi_c = 0. \tag{4.11}$$

It is possible to determine ψ_c by integration of (4.11) with the result

$$\psi_c = \psi_\Gamma \frac{1-y}{1-Y}, \tag{4.12}$$

where the value of the streamfunction on the interface ψ_Γ and the contour function Y depend on the transverse coordinate z. For the derivation of this result we used the condition of periodicity, i.e. symmetry with respect to $y = 1$. Since no fluid crosses the line $y = 1$ this line is a streamline. Its constant value is continuously matched with the symmetry condition $\psi_c(z = 0) = 0$ so that $\psi_c(y = 1) = 0$.

The pressure gradient in the core is obtained with Ohm's law (2.15) as $\partial_z p = j_x = -\partial_x \phi - w_c$ which gives

$$\partial_z p \approx -\frac{1}{1-Y}\psi_\Gamma \text{ near } \Gamma. \tag{4.13}$$

This relation neglects small axial potential gradients $\partial_x \phi = O(z/d)$ since $d \gg z_p$.

4.3. *The interface*

It has been shown in a number of studies that the pressure is uniform along magnetic field lines and does not vary across the Hartmann layer at the leading order of approximation (see e.g. Moreau 1990). This means that the core pressure calculated from (4.13) can be taken as the liquid pressure at the interface. We assumed above that the vapour conditions are uniform in the cross-section of the vapour channel so that the pressure of the vapour p_v at the interface and the inertial contributions are constant in the cross-section considered. This leads to a pressure difference between the vapour and the liquid that varies along the interface. This varying difference in pressure can be balanced only by a varying curvature along the interface. If we project the interface condition (2.3) onto the direction normal to the interface and differentiate with respect to z we find

$$\partial_z p + T\partial_z K = 0 + O(Ha^{-2}), \tag{4.14}$$

where, in the present notation, T stands for the surface tension scaled by $\sigma v_0 B^2 L^2$ and K is twice the non-dimensional mean curvature. We eliminate the pressure using

https://doi.org/10.1017/S0022112002002136 Published online by Cambridge University Press

(4.13), describe the contour as $Y = R(\varphi)\cos\varphi$ in cylindrical coordinates and express curvature and transverse derivative as

$$K = \frac{R^2 + 2R'^2 - RR''}{(R^2 + R'^2)^{3/2}} \tag{4.15}$$

and

$$\partial_z = \frac{1}{R\cos\varphi}\partial_\varphi. \tag{4.16}$$

We know further that ψ_Γ is proportional to the arclength measured along the contour

$$\psi_\Gamma = -\int \sqrt{R^2 + R'^2}\,\mathrm{d}\varphi. \tag{4.17}$$

After all substitutions and additional differentiation with respect to φ we obtain the equation

$$-\sqrt{R^2 + R'^2} = T\partial_\varphi\left(\frac{1 - R\cos\varphi}{R\cos\varphi}\partial_\varphi K\right), \tag{4.18}$$

which determines the contour in a horizontal plane. This equation is solved with boundary conditions

$$R(0) = R_0, \quad R'(0) = 0, \quad R'''(0) = 0, \quad R'(\pi/2) = 0. \tag{4.19}$$

The value of R_0 determines the size of the vapour channel measured along magnetic field lines. The conditions that $R'(0) = R'(\pi/2) = 0$ result from symmetry with respect to the y- and z-axes. The symmetry of the pressure field with respect to the y-axis requires $R'''(0) = 0$. For strong magnetic fields the channels will become highly elongated along the field lines. Then, $R'(\pi/2) = 0$ loses its physical relevance. The solution of (4.18) is meaningful only up to the position φ_1, where the contour has a vertical tangent given by

$$R'\sin\varphi_1 + R\cos\varphi_1 = 0. \tag{4.20}$$

The solution for the contour has then to be completed by a vertical straight line. Since the curvature of this line is zero, there is no jump in pressure across the interface along the line. Therefore, at the point where the straight line meets the solution of (4.18) a jump in pressure has to be excluded. This requires that the curvature calculated from $R(\varphi)$ also vanishes at $\varphi = \varphi_1$,

$$R^2 + 2R'^2 - RR'' = 0 \quad \text{at} \quad \varphi = \varphi_1. \tag{4.21}$$

The solution of (4.18) is obtained numerically by using MAPLE routines with initial conditions

$$R(0) = R_0, \quad R'(0) = 0, \quad R''(0) = \alpha, \quad R'''(0) = 0. \tag{4.22}$$

The shooting parameter α is chosen such that either all conditions in (4.19) are satisfied or if a vertical tangent appears at $\varphi_1 < \pi/2$ we chose α such that (4.21) is satisfied, i.e. that the curvature vanishes at φ_1.

The resulting contours of the vapour channels are displayed in figure 7. If the surface tension dominates magnetic forces, when $T/R_0^3 \gg 1$, the shapes of vapour channels are circular. The vapour cross-sections start to become elongated along field lines if both forces become comparable. For $T/R_0^3 \ll 1$ the elongation is dominant and contours become possible where a major part of the interface is straight and aligned with the field. The maximum width of such channels seems to be proportional to $T^{1/3}$ for small T.

https://doi.org/10.1017/S0022112002002136 Published online by Cambridge University Press

$$\rho = 414\,\mathrm{kg\,m^{-3}}, \quad \nu = 4.2 \times 10^{-7}\,\mathrm{m^2\,s^{-1}}, \quad \sigma = 1.8 \times 10^{6}\,\Omega^{-1}\,\mathrm{m^{-1}}$$
$$\rho_v = 0.021\,\mathrm{kg\,m^{-3}}, \quad \nu_v = 7 \times 10^{-4}\,\mathrm{m^2\,s^{-1}}, \quad H = 2.0 \times 10^{7}\,\mathrm{J\,kg^{-1}}, \quad \gamma = 0.237\,\mathrm{N\,m^{-1}}$$
$$q = 20 \times 10^{6}\,\mathrm{W\,m^{-3}}, \quad B = 10\,\mathrm{T}, \quad a = 1$$

TABLE 1. Properties of lithium and operating condition for EVOLVE.

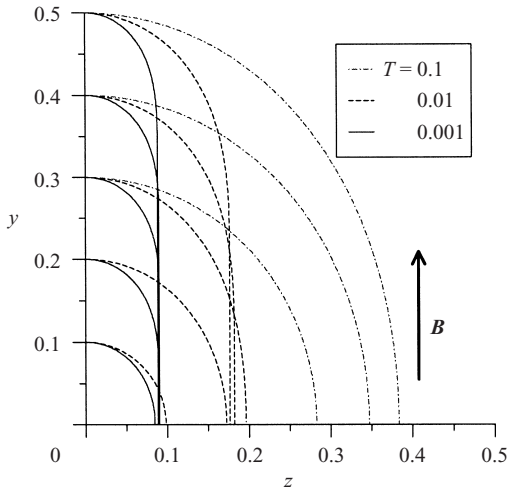


FIGURE 7. Shapes of vapour channels for different values of surface tension and channel size.

In order to obtain an impression of typical values of parameters involved we introduce the physical data of the EVOLVE concept as shown in table 1. Such conditions lead e.g. for $R_0 = 0.3$ to $v_0 = qaL^2(\rho H l)^{-1} = 5 \times 10^{-5}\,\mathrm{m\,s^{-1}}$, $Ha = LB\sqrt{\sigma/\rho\nu} = 10^4$, and $T = \gamma(\sigma v_0 B^2 L^2)^{-1} = 0.25$ for $L = 0.01\,\mathrm{m}$ so that the expected contour is elliptical rather than highly elongated. However, if the spacing between vapour channels is chosen larger, or if it turns out that the magnetic field which is required for a safe confinement of the fusions plasma should be larger, then T could even reach values for which highly elongated vapour columns become possible.

4.4. *Flow pattern*

In § 4.3 we determined the shape of the interface, $R(\varphi)$. These results determine the streamfunction along the vapour–liquid interface according to (4.17) and yield with (4.12) the flow field outside the viscous layers. Results are displayed in figure 8 which shows streamlines towards vapour channels. The length of the channels along field lines is $R_0 = 0.3$ and the surface tension parameters are $T = 0.1$, 0.01 and 0.001. Cases with larger values of T do not differ qualitatively from results shown here for $T = 0.1$. In all cases internal parallel layers develop along the magnetic field line which is tangential to the contour of the vapour channel at $z = z_p$. To the right of the parallel layer for $z > z_p$ the flow is parallel and oriented perpendicular to the magnetic field. The velocity is uniform along field lines with equidistant isolines of the streamfunction. To the left of the parallel layer for $0 < z < z_p$ the streamlines have a shape similar to hyperbolae centred at $y = 1$, $z = 0$. For $T = 0.1$ and 0.01 the solutions to the right and to the left are continuous across the parallel layer but exhibit discontinuous slopes at $z = z_p$. Here the role of the internal layer is

https://doi.org/10.1017/S0022112002002136 Published online by Cambridge University Press

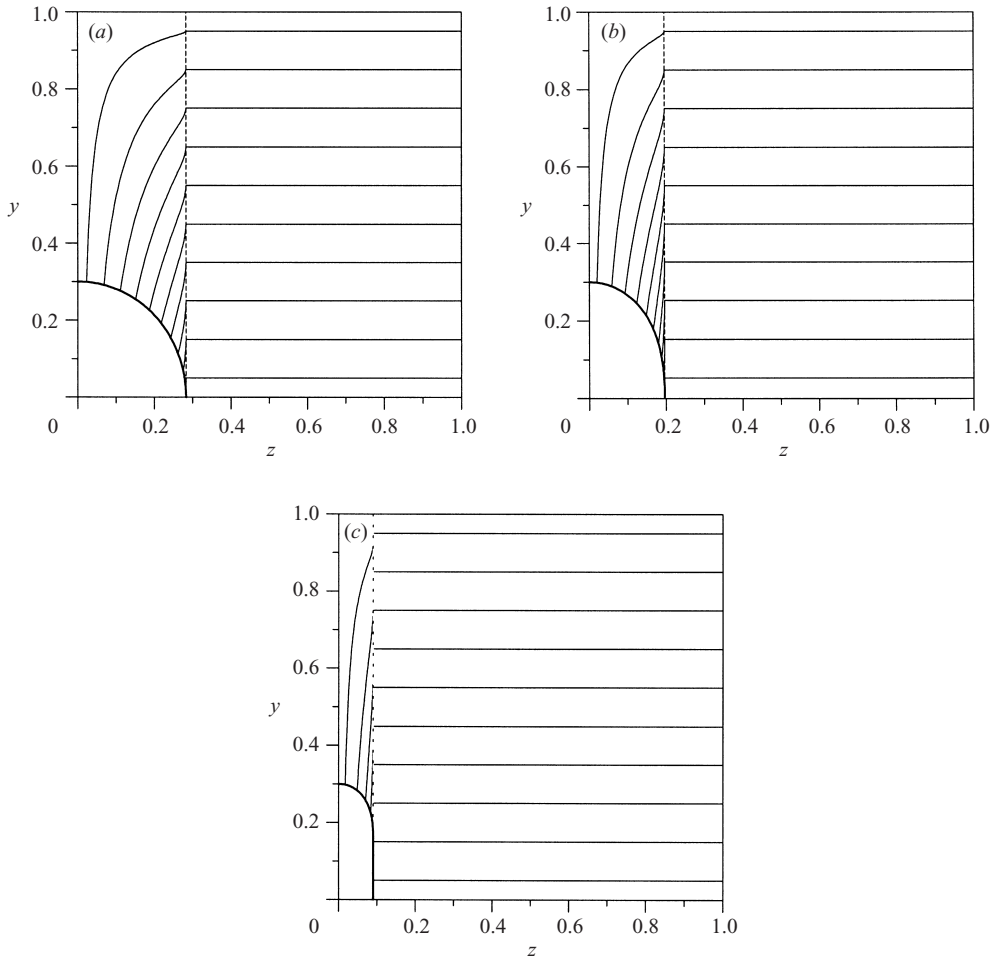


FIGURE 8. Streamlines for $R_0 = 0.3$ and (*a*) $T = 0.1$, (*b*) $T = 0.01$, (*c*) $T = 0.001$.

quite passive since it smooths only the discontinuous y-component of velocity. For $T = 0.001$ the situation is different. Here we have a contour which is aligned with the field not only at one point but along a large portion of the surface. All liquid which crosses the parallel portion of the interface is carried by the parallel layer along field lines. An $O(1)$ flow rate carried within a layer of thickness $\delta_p \sim Ha^{-1/2}$ requires a high-velocity jet with velocities on the order $v \sim Ha^{1/2}$. This is why in figure 8(*c*) the core streamfunction becomes discontinuous across the parallel layer. Parallel layers similar to the present one occur in buoyant magneto-convection in horizontal Bridgman crystal growth as reported by Garandet *et al.* (1992). These authors find, as we do in the present case, a flow with parallel streamlines oriented perpendicular to the magnetic field at some distance from the parallel layer. Within a layer of thickness $\delta_p \sim Ha^{-1/2}$ the flow is redistributed in a high-velocity jet near a wall aligned with the magnetic field. If details of the flow in the internal parallel layer are required it should be possible to reconstruct such a flow from the solutions in both cores (see e.g. Garandet *et al.* 1992).

In order to confirm the results obtained by the asymptotic analysis we compare streamlines with those obtained by a numerical solution at a large Hartmann number.

https://doi.org/10.1017/S0022112002002136 Published online by Cambridge University Press

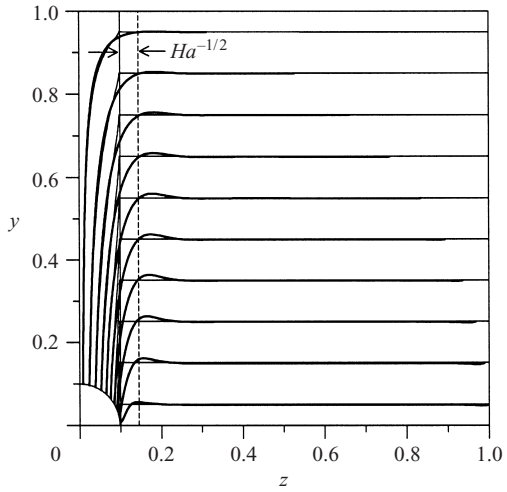


FIGURE 9. Streamlines calculated from a numerical solution (thick) compared with those obtained by the asymptotic analysis (thin) for $Ha = 500$, $R_0 = 0.1$ and $T = 0.01$.

The most simple comparison is possible for a case where the shape of the interface is nearly circular. This allows us to use the same numerical procedure as outlined above for which we used the polar coordinate system. Only the inflow conditions are different. Instead of (3.9) we now have a uniform inflow perpendicular to the applied magnetic field. In terms of the streamfunction the inflow condition becomes

$$\psi = R_0 \frac{\pi}{2} (\cos\varphi - 1), \quad \omega = 0 \quad \text{at} \quad r = 1, \tag{4.23}$$

while the condition at the interface

$$\psi = -R_0\varphi, \quad \omega = 0 \quad \text{at} \quad r = R_0, \tag{4.24}$$

is now posed at a radius $R_0 < 1$ due to the different scaling of the problem. In the present problem the Hartmann number is $Ha = 500$. A comparison shows a good agreement of both solutions at some distance from the internal parallel layer of thickness $\delta_p \sim O(Ha^{-1/2})$. The comparison of streamlines is shown in figure 9.

4.5. *Three-dimensional considerations*

We assumed above that the two-dimensional flow in horizontal planes perpendicular to the vapour channels is driven by a pressure gradient. A driving pressure gradient, however, could be maintained only by the hydrostatic pressure head due to an inclination of the free surface of the liquid pool. The two-dimensional assumption would be valid if the non-dimensional liquid depth d is much larger than the width of vapour channels, i.e. for $d \gg z_p$. We observed currents which are perpendicular to the horizontal plane, with a direction parallel to the vapour channels. At the bottom of the tray the currents may enter or leave the electrically conducting solid wall and close their path within the wall. The situation is schematically shown in figure 10 which displays a vertical plane through a vapour channel. A closure of currents must be established within the fluid since the ambient medium on top of the liquid layer is electrically insulating. For that reason a current component j_z along z is required in addition to the current component j_x. While the Lorentz forces f_z oppose the fluid motion, the Lorentz forces f_x have a direction perpendicular to the free surface. The

https://doi.org/10.1017/S0022112002002136 Published online by Cambridge University Press

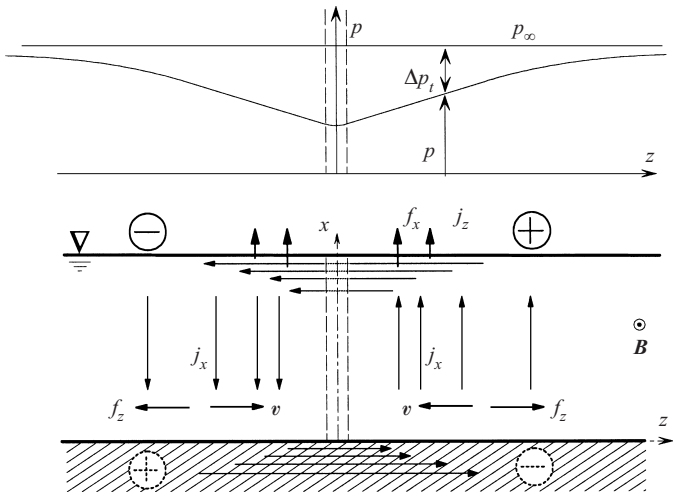


FIGURE 10. Sketch of current paths, Lorentz forces and pressure distribution.

latter Lorentz forces decrease the pressure gradually from the surface where $p = p_\infty$ to the core value p. We will show below that the pressure difference Δp_t due to f_x, which gives an additional forcing to drive the flow towards the vapour channel, balances at least partly the MHD pressure drop. At leading order, a balance of momentum in the cores is given by

$$\left.\begin{aligned} \partial_z p &= j_x = \partial_z \Psi, \\ \partial_x p + G &= -j_z = \partial_x \Psi, \end{aligned}\right\} \tag{4.25}$$

where Ψ is a streamfunction for electric currents in the (x, z)-plane. We have seen above that variables do not vary along magnetic field lines and that currents j_y are absent in the cores. Most of the liquid region is occupied by core II so that we focus the following analysis on this region. It is to be expected that results in core I are quite similar as long as the vapour channel cross-section remains small. A balance of charge in a volume element is

$$\partial_x j_x + \partial_z j_z = 0 \tag{4.26}$$

and it is satisfied identically by the use of Ψ. We further know that the top surface is insulating. This requires that the surface contour is a current streamline with $\Psi =$ constant, i.e.

$$\begin{aligned} \mathrm{d}\Psi &= \partial_x \Psi \,\mathrm{d}x + \partial_z \Psi \,\mathrm{d}z \\ &= \mathrm{d}p + G\,\mathrm{d}x = 0. \end{aligned} \tag{4.27}$$

At the free surface there is a uniform pressure p_∞ with $\mathrm{d}p = 0$. This requires that $\mathrm{d}x = 0$, a condition which demands a flat and horizontal top surface. We regain by this mechanism the energy which has been lost by magnetic braking in the core. The core extracts mechanical energy from the system and converts it into electrical energy. This is carried to other places where it is released in order to keep the surface elevation roughly constant instead of highly inclined towards the channels.

There is another point that should be stressed in the present discussion. The currents which flow in the horizontal direction require a driving potential gradient, both near the top and at the bottom as indicated by the symbols $\oplus$ and $\ominus$ in figure 10. This leads to the formation of a vertical potential gradient $\partial_x \phi$ as well, which, at large distance

https://doi.org/10.1017/S0022112002002136 Published online by Cambridge University Press

from the vapour channel, balances the induced electric field. As a consequence the currents, the Lorentz forces, and the MHD pressure drop vanish when $\partial_x\phi \to -w$ as $z \to \pm\infty$. However, there remain differences in comparison with known free-surface flows in open channels (see e.g. Molokov & Reed 1999) since Hartmann walls are absent due to the assumed periodicity along y.

If we want to account for three-dimensional effects and describe the current path but intend to stay within the two-dimensional assumptions for the fluid flow we have to solve the equations for the electric potential. We chose a general representation of potential in the core in terms of a Fourier series as

$$\phi = -w\frac{x^2}{2d} + \sum_{i=1} \phi_i(z)\sin(\lambda_i x), \quad \text{with} \quad \lambda_i = \frac{\pi}{2d}(2i-1), \tag{4.28}$$

valid for a perfectly conducting bottom wall. The values of ϕ_i depend on z only and d is the non-dimensional depth of the liquid layer. A dependence of ϕ_i on the y-coordinate is excluded due to Ohm's law and symmetry with respect to $y = 0$. With this representation of potential (2.15) is now

$$\left.\begin{aligned} j_x &= -\partial_x\phi - w = -w\left(1 - \frac{x}{d}\right) - \sum \lambda_i\phi_i\cos(\lambda_i x), \\ j_z &= -\partial_z\phi + u \approx \partial_z w\frac{x^2}{2d} - \sum \partial_z\phi_i\sin(\lambda_i x). \end{aligned}\right\} \tag{4.29}$$

With these currents (4.26) leads to

$$\sum(\partial_{zz}\phi_i - \lambda_i^2\phi_i)\sin(\lambda_i x) = \frac{1}{d}\left(w + \partial_{zz}w\frac{x^2}{2}\right). \tag{4.30}$$

Using orthogonality of trigonometric functions we find the following equations determining the unknown potential coefficients:

$$\partial_{zz}\phi_i - \lambda_i^2\phi_i = \frac{2}{d^2}\int_0^d \left(w + \partial_{zz}w\frac{x^2}{2}\right)\sin(\lambda_i x)\,\mathrm{d}x. \tag{4.31}$$

For core II we have w = constant so that we find a solution that does not grow exponentially as $z \to \infty$:

$$\phi_i = \frac{-2w}{d^2\lambda_i^3} + c_i\exp(-\lambda_i z) \quad \text{for} \quad z > z_p. \tag{4.32}$$

The constants of integration c_i could be evaluated by matching with an exact solution of the problem for $z < z_p$. We shall not do that. However, symmetry with respect to the x-axis requires that ϕ vanishes at $z = 0$. Since the solution near $z = 0$ is continuous and smooth we assume that deviations from (4.32) are small for $z_p \ll 1$. This assumption allows us to apply the symmetry condition at $z = 0$ directly to (4.32) and to determine c_i approximately.

Isolines of potential and streamlines of electric currents are shown in figure 11. As $z \to \infty$ the isolines of potential become equidistant, i.e. a uniform axial electric field balances the induced electric field so that currents and associated Lorentz forces vanish. The currents close within the core with the consequence that the top surface layer is more or less passive.

We can now estimate the axial component of the electric potential gradient near the vapour channel. An evaluation of $\partial_x\phi$ shows that the leading terms near $z = 0$ are proportional to $\partial_x\phi \sim z/d$, a quantity that is negligible for $d \gg z$. This especially holds

https://doi.org/10.1017/S0022112002002136 Published online by Cambridge University Press

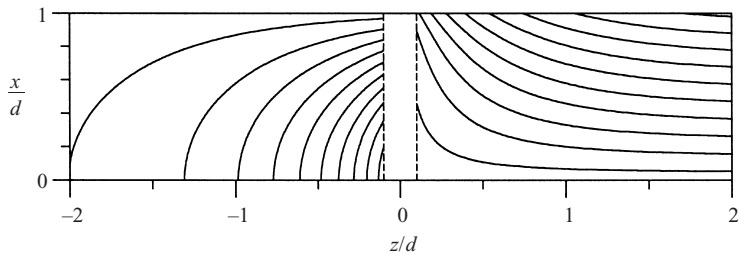


FIGURE 11. Streamlines of electric currents (left) and isolines of potential (right).

near the liquid–vapour interface where there are small values of z, i.e. $z < z_p < 1$. This justifies the assumption made for the determination of the interfacial shape, where $\partial_x \phi$ had been neglected.

The solution derived above was based on the assumption that the bottom wall is perfectly conducting. If that wall were insulating we would have to take d as the half-height of the liquid layer and show results in a domain $-d < x < d$.

More accurate results require a detailed three-dimensional analysis which is outside the scope of the present work.

5. Conclusions

The magnetohydrodynamic flow in the liquid phase for a specific pool boiling scenario proposed for the EVOLVE concept of a fusion blanket has been investigated. In the EVOLVE concept one possible boiling scenario in horizontal layers of liquid lithium is based on the formation of permanent vertical vapour channels at the surfaces of which the heat is removed by evaporation. Numerical and asymptotic analyses show that near the vapour channels the flow is mainly parallel to the applied magnetic field. Depending on the inflow conditions the parallel layers that spread along the field lines which are tangential to the vapour channel become more or less important. In particular, for the case when the channels have a periodic occurrence along field lines the liquid must be supplied from a direction perpendicular to the magnetic field. Then, at large distance from the vapour channel the flow has a uniform velocity with equidistant streamlines. When the liquid approaches the parallel layer the flow turns and follows streamlines with a hyperbola-like shape before it reaches the liquid–vapour interface. Depending on the surface tension parameter and the size of the vapour channel the interface may be elongated along field lines or remain circular. The proof that such a boiling scenario is possible was not the subject of the present work and remains to be found.

Appendix. Vapour flow and geometry of a capillary

We assumed above that the cross-sections of vapour channels vary slowly along the axis so that the flow towards the vapour–liquid interface can be considered to be two-dimensional in horizontal planes. In order to justify this assumption let us consider the hydrodynamic case and estimate the size of a vapour column in which we consider the vapour to be incompressible. Such an assumption has been used e.g. by Koh (1962) for the determination of the vapour flow near a heated wall. For details of the geometry see figure 2. We assume further that the heat per unit length of the capillary removed by evaporation at the interface is constant, i.e. $Q_x = \text{constant}$.

https://doi.org/10.1017/S0022112002002136 Published online by Cambridge University Press

The mass transfer at the interface is then fixed by $H\rho_v(\boldsymbol{v}_v \cdot \hat{\boldsymbol{r}})2\pi R = -Q_x$, where H stands for the latent heat of vapourization and $\hat{\boldsymbol{r}}$ is the radial unit vector. A balance of axial momentum of the stationary vapour flow in a slender vapour channel yields, in cylindrical coordinates,

$$\left[\boldsymbol{v}_v \cdot \nabla - \nu_v \frac{1}{r}\partial_r(r\partial_r)\right](\boldsymbol{v}_v \cdot \hat{\boldsymbol{x}}) = -\frac{1}{\rho_v}\partial_x p_v - g. \tag{A 1}$$

We satisfy mass conservation by using a velocity streamfunction:

$$\boldsymbol{v}_v = -\frac{1}{r}\partial_r \psi \hat{\boldsymbol{x}} + \frac{1}{r}\partial_x \psi \hat{\boldsymbol{r}}, \tag{A 2}$$

and apply a self-similar transformation according to

$$\psi = V f(\eta) x \quad \text{with} \quad \eta = \frac{r}{R(x)}. \tag{A 3}$$

The linear dependence of ψ on x and the magnitude $V = \boldsymbol{v}_v \cdot \hat{\boldsymbol{r}}\, R = (1/2\pi)(Q_x/\rho_v H)$ are determined by the mass flux condition at the interface. We substitute the latter definitions into (A 1) and eliminate the pressure by using (2.3) and (2.4). Unfortunately we are unable to balance all terms simultaneously by choosing a suitable radius $R(x)$. We may distinguish two regimes. In the capillary regime, the radius of the vapour channel is relatively small, and capillary forces dominate the hydrostatic pressure force of the liquid so that we may neglect the latter. In this regime a balance of inertia, viscous and capillary forces determines $R(x)$ in the first part of a developing capillary. The radius of the capillary grows with increasing length. For longer capillaries, capillary forces decrease while the hydrostatic force increases.

At a certain length we find a dominant balance of forces by an equilibrium between hydrostatic force, inertia and viscous forces. This regime permits a self-similar solution with

$$R(x) = d\varepsilon(X) \quad \text{with} \quad X = x/d. \tag{A 4}$$

Here d stands for a typical length of the capillary and ε is the aspect ratio (radius/depth of the liquid layer). For a comparison of gravity forces with capillary forces we introduce a Bond number

$$Bo = \frac{(\rho - \rho_v)g d^2}{\gamma}. \tag{A 5}$$

Using this non-dimensional number, the ratio of gravity forces to capillary forces becomes proportional to $\varepsilon\, Bo$. Self-similar solutions apply exactly for $Bo \to \infty$ and for $\varepsilon = \hat{\varepsilon} X^{1/4}$. Here, $\hat{\varepsilon}$ corresponds to the final radius of the capillary. The solution

$$f(\eta) = \eta^4 - 2\eta^2 \tag{A 6}$$

satisfies with (A 4) the mass flux condition at the interface and the symmetry conditions on the axis. This representation of the streamfunction describes an axial velocity profile with parabolic variation along the radial direction. At the liquid–vapour interface the axial component of velocity is zero. Shear stress in the vapour would induce tangential flow in the liquid and so the latter condition, $\boldsymbol{v}_v \cdot \hat{\boldsymbol{x}} = 0$, is not the exact interface condition. However, as shown by Koh (1962) axial liquid velocities become negligible if $(\rho_v^2 v_v/\rho^2 v)^{1/2}$ is small. For EVOLVE it is 6.4×10^{-4} so that the approximation of zero axial interfacial flow is justified. Using ε and f as introduced

https://doi.org/10.1017/S0022112002002136 Published online by Cambridge University Press

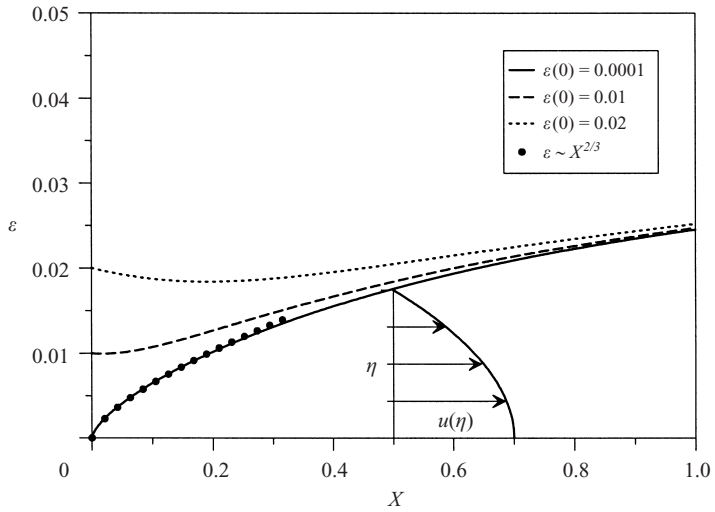


FIGURE 12. Possible contours of vapour capillaries in EVOLVE depending on the initial size of the nucleation site.

above reduces the momentum balance in the vapour, (A 1), with (2.3) and (2.4) to

$$\hat{\varepsilon}^4 = \left(\frac{16}{Re} + 8\right) Fr. \tag{A 7}$$

Here the Reynolds number $Re = V/\nu_v$ measures the ratio of inertia forces to viscous forces for the flow in the vapour channel and the group $Fr = V^2\rho_v/[d^3(\rho - \rho_v)g]$ is a Froude number that compares inertia forces in the vapour with the hydrostatic pressure force. Equation (A 7) determines the magnitude of ε and we find

$$\varepsilon = \left[\left(\frac{16}{Re} + 8\right) Fr\, X\right]^{1/4}. \tag{A 8}$$

As an example we introduce the EVOLVE data according to table 1 and find capillaries of aspect ratio $\hat{\varepsilon} = 0.027$ for $d = 0.05$ m. The variation of the radius with the axial distance, i.e. $\partial_x R$, is on the order $\hat{\varepsilon}$, which suggests a quasi-two-dimensional analysis where we neglect ∂_x in comparison with ∂_y, ∂_z.

For EVOLVE the parameter εBo is near unity so that capillary forces are comparable with hydrostatic forces. Using the same streamfunction as before, we are unable to balance momentum at each point of the cross-section exactly. However, if we consider the momentum equation in a cross-section-averaged sense we can derive an equation which determines the shape of the cross-section by

$$\frac{\varepsilon^4}{X} = \left(\frac{16}{Re} + \frac{32}{3}\right) Fr - \frac{\partial\varepsilon}{\partial X}\left(\frac{1}{Bo}\frac{\varepsilon^2}{X} + \frac{32}{3} Fr \frac{X}{\varepsilon}\right). \tag{A 9}$$

For $Bo \to \infty$ and $\varepsilon = \hat{\varepsilon} X^{1/4}$ (A 9) is consistent with (A 7). We solve this equation numerically, again for the EVOLVE data. Results are shown in figure 12. Depending on the initial size of the nucleation site we obtain capillaries which expand first like $\varepsilon \sim X^{2/3}$ or capillaries which are closer to a cylinder, with only weak changes along X. The analysis derived in the present paper applies best for the latter type of vapour channel.

https://doi.org/10.1017/S0022112002002136 Published online by Cambridge University Press

REFERENCES

Abdou, M. A. & The Apex Team 2001 On the exploration of innovative concepts for fusion chamber technology. *Fusion Engng Design* **54**, 181–247.

Anderson, M. H., Murphy, J. G., Sawan, M. E., Sviatoslavsky, I. N., Corradini, M. L. & Malang, S. 2001 EVOLVE lithium tray thermal-hydraulic analysis. *Fusion Technol.* **39**, 810–814.

Davidson, P. A. 2001 *An Introduction to Magnetohydrodynamics*. Cambridge University Press.

Dwyer, O. E. 1976 *Boiling Liquid-Metal Heat Transfer*. Hinsdale, Illinois: American Nuclear Society.

Garandet, J., Alboussiere, T. & Moreau, R. 1992 Buoyancy driven convection in a rectangular enclosure with a transverse magnetic field. *Intl J. Heat Mass Transfer* **35**, 741–748.

Hsieh, D. Y. 1972 Effects of heat and mass transfer on Rayleigh–Taylor instability. *Trans. ASME* D: *J. Basic Engng* **94**, 156–158.

Hunt, J. C. R. & Leibovich, S. 1967 Magnetohydrodynamic flow in channels of variable cross-section with strong transverse magnetic fields. *J. Fluid Mech.* **28**, 241–260.

Kern, M., Berger, P. & Hügel, H. 2000 Magneto-fluid dynamic control of seam quality in CO_2 laser beam welding. *Welding J.* **79**(3), 72s–78s.

Koh, J. C. Y. 1962 Analysis of film boiling on vertical surfaces. *J. Heat Transfer* **84**, 55–62.

Lopez de Bertodano, M. A., Leonardi, S. & Lykoudis, P. S. 1998 Nucleate pool boiling of mercury in the presence of magnetic field. *Intl J. Heat Mass Transfer* **41**, 3491–3500.

Molokov, S. & Reed, C. B. 1999 Review of free-surface MHD experiments and modelling. *Tech. Rep.* ANL/TD/TM99-08. Argonne National Laboratory.

Moreau, R. 1990 *Magnetohydrodynamics*. Kluwer.

Müller, U. & Bühler, L. 2001 *Magnetofluiddynamics in Channels and Containers*. Springer.

Tse, H. C., Man, H. C. & Yue, T. M. 1999 Effect of magnetic field on plasma control during CO2 laser welding. *Optics Laser Technol.* **31**, 363–368.

Whalley, P. B. 1987 *Boiling, Condensation and Gas–Liquid Flows*. Clarendon.

https://doi.org/10.1017/S0022112002002136 Published online by Cambridge University Press